THE BEHAVIOR OF RESIDUAL STRESS UNDER CYCLIC THERMO-MECHANICAL LOADS IN AUTOFRETTAGED AND SHRINK-FITTED CYLINDERS

Ossama R. Abdelsalam
Lecturer, Department of Weapons and Ammunition, Military Technical College, Cairo, Egypt
Email: ossama.ramy@mtc.edu.eg

ABSTRACT

The autofrettage and shrink-fit processes are used to create compressive residual stresses at the near bore area to increase the load-bearing capacity of the pressure vessels under thermomechanical loads. In this paper, an investigation of the effect of thermal accumulation due to cyclic thermomechanical loads on the residual stresses created by autofrettage and shrink-fit processes has been revealed. A Fully coupled thermo-elastic finite element model has been developed in ANSYS environment to calculate the temperature, hoop, and equivalent von –Mises stresses profiles through the wall thickness of the cylinder. The finite element model is utilized to illustrate the behavior of the residual stresses after different cyclic regimes of thermomechanical loads considering thermal accumulation. It has been found that relaxation time within 60 seconds as a minimum is crucial after a certain number of thermo-mechanical loads to let the cylinder withstand more thermomechanical cycles.

INTRODUCTION

Gun barrels, nuclear reactors, chemical plants, food reserving have severe cyclic thermo-mechanical loading conditions. The cylindrical shell is one of the most pervasive machinery used in these applications. In order to increase pressure and thermal capacities or even to reduce the heaviness of these cylindrical shells, researchers have tried to manage these limitations by designing cylinders exposed to shrink-fit [1-2], autofrettage techniques, or combined of them [3-8]. The main objective in both shrink-fit and autofrettage techniques is to create beneficial compressive residual hoop stresses in the near-bore zone of the cylindrical shell. However, there is still an open question here regarding the durability of these cylinders under these cyclic thermo-mechanical loads consider thermal accumulation. In other words, there is a lake in the researches about the behavior of these residual stresses created by shrink–fit or autofrettage processes under the effect of thermal accumulation created due to the cyclic thermo-mechanical loads.

Some researchers used thermo-mechanical loads to create the residual stresses in the cylinders. Mohan et al. studied the fatigue life of a thick cylinder under thermal autofrettage with shrink-fit to increase the carrying load capacity [9]. R.Shufen et al. strengthened his cylinder after thermal autofrettage by heat treatment. He could retain beneficial compressive residual stresses at both the inner and outer walls of the cylinder [10]. S. M. Kamal et al. compared the thermal autofrettage with the conventional hydraulic autofrettage out considering various aspects. He found that thermal autofrettage, the maximum possible pressure carrying capacity increases with the wall thickness ratio. He also investigated autofrettaged cylinders subjected to combined thermal gradient and pressure loading simultaneously, but he observed that the suitability of one process over the other will depend on the actual magnitudes of thermal gradient and pressure [11]. On the other hand, some researchers studied the effect of thermo-mechanical loads on the residual stresses created in mechanical structures due to welding, peening processes. Xue-fang Xie et al. studied the relaxation of weld residual stress in a 316L stainless steel weld joint under cyclic loading by experiments and FEM. They found that the more increase of the number of cycles and stress amplitude the more weld residual stresses are released [12]. S. A. Meguid et al. created a F.E.M to model the shot-peening process and the induced residual stresses. They also modeled the influence of thermo-mechanical cyclic overload on residual stress relaxation. They found that the cyclic thermo-mechanical loads increase the applied tensile coincides with a decrease in the yield stress of the material due to exposure to an elevated temperature, with a greater resulting relaxation of residual stresses induced by the peening process [13]. This study attempts to explore the influence of thermo-mechanical cyclic loads on the residual stress induced in autofrettaged and shrink-fitted cylinders considering thermal accumulation. At first, a 3D FEM is developed to evaluate the residual stresses in both autofrettage and 2-layer shrink-fit cylinders. Then, a sequential coupling 3D transient thermo-mechanical FEM was established to study the stress distribution under the effect of cyclic thermo-mechanical loads showing the behavior of the residual stresses after these loads. Also, the effect of relaxation cooling time on the residual stresses has been observed.

FINITE ELEMENT MODEL

Two FE models have been constructed in the environment of ANSYS 18 WORKBENCH as shown in Figures 1, 2. They have been used to calculate the residual hoop stresses for the autofrettaged mono-block cylinder and the two layers shrink fitted cylinder, respectively. The chosen element has brick geometry with 20 nodes and three degrees of freedom at each node. The element has plasticity and large strain capabilities and can provide many outputs such as deformations, stresses, strains, temperature, and total plastic strain [14]. The general dimensions of the two cylinders are the same with a length of L=2 m, inner radius of a= 100 mm the outer radius b=200 mm.

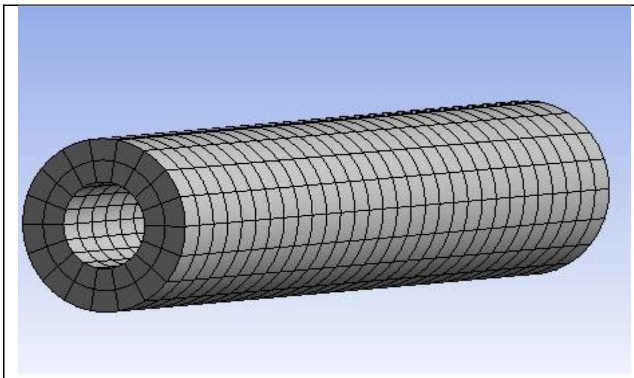

Figure 1. Geometric and finite element model of mono-block autofrettaged cylinder.

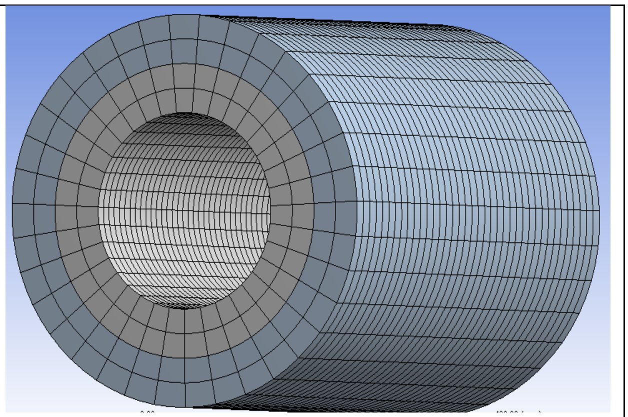

Figure 2. Geometric and finite element model of the two-layered shrink-fitted cylinder.

For the autofrettaged mono-block cylinder, the bilinear kinematic hardening FEM has been validated by comparing the results with published work [15], as shown in Figure 3. The mono-block cylinder made of (NiCrMoV125) steel has inner and outer radii of a= 146 mm and b=305 mm, the residual stress has been calculated after performing 700 MPa autofrettage pressure.

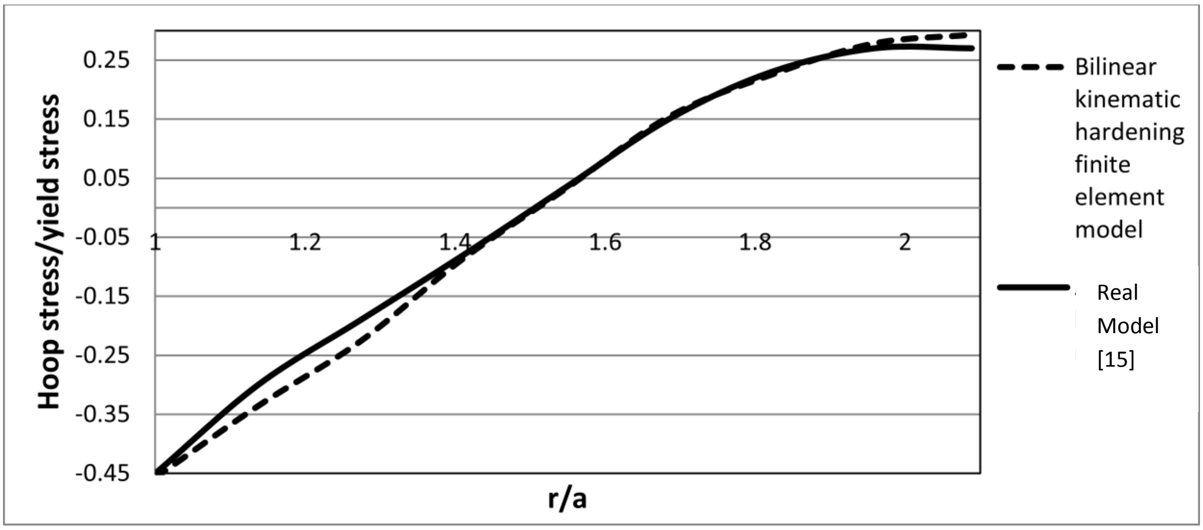

Figure 3. Residual hoop stress for a mono-block autofrettage cylinder using the bilinear kinematic hardening and the real models.

Nevertheless, the residual stress due to shrink-fit for the two-layer cylinder is compared with the available analytical solution [16]. The interference pressure P_{sh} developed between the shrink-fitted cylinders and the residual hoop σ_θ stresses along the radial position r for inner and outer cylinders can be calculated as:

$$P_{sh} = \frac{0.5\,\delta}{\frac{c}{E_o}\left(\frac{b^2+c^2}{b^2-c^2}+\upsilon_o\right)+\frac{c}{E_i}\left(\frac{a^2+c^2}{c^2-a^2}-\upsilon_i\right)} \qquad (1)$$

$$\sigma_{\theta_{inner}} = -P_{sh}\frac{c^2}{c^2-a^2}\left(1+\frac{a^2}{r^2}\right) \qquad (2)$$

$$\sigma_{\theta_{outer}} = P_{sh}\frac{c^2}{b^2-c^2}\left(1+\frac{b^2}{r^2}\right) \qquad (3)$$

Where δ is the total radial interference, a and b are inner and outer radii, c is interference radius, E_i, E_o and υ_i, υ_o are the modulus of elasticity and the Poisson's ratio of inner and outer cylinders materials, respectively.

The distribution of the residual hoop stresses through the wall thickness has been evaluated by the FEM and analytically, as shown in Figure 4. In this cylinder, both layers are made from the same material same as the material used in the autofrettaged cylinder. The cylinder has inner, outer, and interference radii of 100, 200, 150 mm respectively, and the radial interference is 0.44 mm.

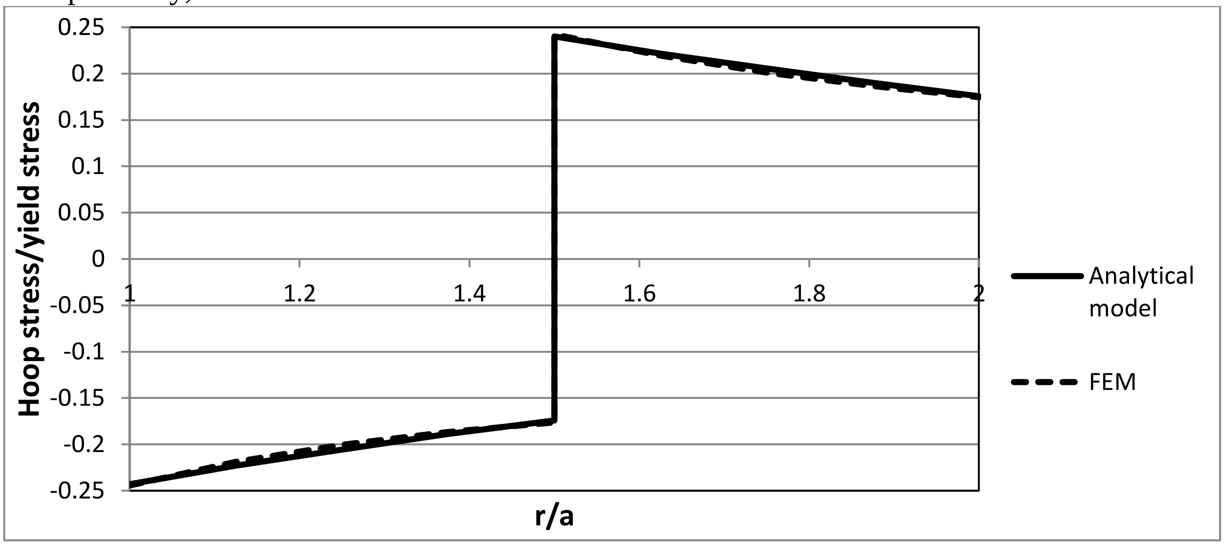

Figure 4. Residual hoop stress distribution for a two-layer shrink-fit cylinder

In Figures 3 and 4, r is the radial position. As it can be seen, the predicted residual hoop stresses based on FEM agree well with the residual stress of the actual measured material behavior in the autofrettaged cylinder and the analytical residual stress of the shrink-fit cylinder.

FULLY COUPLED THERMO-ELASTIC ANALYSIS

Here, the governing differential equations are first formulated and then cast into the finite element form which is constructed in the ANSYS 18 environment.

3.1. Governing equations

Due to symmetry condition, no shear stresses exist and thus in the absence of body forces, one can write the following governing differential equation in the radial direction as [17, 18]:

$$\frac{\partial\sigma_r}{\partial r} + \frac{\sigma_r-\sigma_\theta}{r} = \rho\ddot{u}_r \qquad (4)$$

In Equation 4 σ_r and σ_θ are radial and hoop stresses and $\ddot{u}_r$ is the radial acceleration.

For long cylindrical shape the assumption of plane strain ($\varepsilon_z = 0$) is effective, the strain-displacement relation can be termed as:

$$\varepsilon_r = \frac{\partial u_r}{\partial r}, \qquad \varepsilon_\theta = \frac{u_r}{r} \qquad (5)$$

Consequently, stress-strain relation using generalized Hook's law bearing in mind thermal effect can be printed as:

$$\sigma_r = \frac{E}{(1+\nu)(1-2\upsilon)}[(1-\nu)\varepsilon_r + \nu\varepsilon_\theta] - \frac{E\alpha}{(1-2\nu)}T \qquad (6)$$

ISSN: 2394-3696 Website: ijiert.org
VOLUME 8, ISSUE 6, June. -2021

$$\sigma_\theta = \frac{E}{(1+\nu)(1-2\nu)}[\nu\varepsilon_r + (1-\nu)\varepsilon_\theta] - \frac{E\alpha}{(1-2\nu)}T \quad (7)$$

Where T (r, t) is the change of temperature difference with radial position r and time t.

Now using the above equations, that yields to governing equation of motion only in terms of displacement:

$$\frac{\partial^2 u_r}{\partial r^2} + \frac{1}{r}\frac{\partial u_r}{\partial r} - \frac{u_r}{r^2} - \frac{\alpha(1+\nu)}{(1-\nu)}\frac{\partial T}{\partial r} - \frac{\rho}{E}\frac{(1+\nu)(1-2\nu)}{(1-\nu)}\ddot{u}_r = 0 \quad (8)$$

On the flip side, the Fourier's transient heat conduction equation for the cylinder can be written as:

$$k\frac{\partial^2 T}{\partial r^2} + k\frac{1}{r}\frac{\partial T}{\partial r} = \rho c_p \frac{\partial T}{\partial t} + \frac{T_o E\alpha}{(1-2\nu)}\left(\frac{\partial \varepsilon_r}{\partial t} + \frac{\partial \varepsilon_\theta}{\partial t}\right) \quad (9)$$

Where k, c_p, and α are the thermal conductivity, specific heat, and thermal expansion coefficient, respectively.

Now using equations 4 and 5 with equation 9, one can obtain:

$$k\frac{\partial^2 T}{\partial r^2} + k\frac{1}{r}\frac{\partial T}{\partial r} = \rho c_p \frac{\partial T}{\partial t} + \frac{T_o E\alpha}{(1-2\nu)}\left(\frac{\partial \dot{u}_r}{\partial t} + \frac{\dot{u}_r}{r}\right) \quad (10)$$

Using finite element technique, one could cast the above governing couple thermo-elastic differential equations into the finite element form as:

$$\begin{bmatrix} [m] & [0] \\ [0] & [0] \end{bmatrix}\begin{Bmatrix} \{\ddot{u}\} \\ \{\ddot{T}\} \end{Bmatrix} + \begin{bmatrix} [0] & [0] \\ [C^{tu}] & [C^t] \end{bmatrix}\begin{Bmatrix} \{\dot{u}\} \\ \{\dot{T}\} \end{Bmatrix} + \begin{bmatrix} [K] & [K^{ut}] \\ [0] & [K^t] \end{bmatrix}\begin{Bmatrix} \{u\} \\ \{T\} \end{Bmatrix} = \begin{Bmatrix} \{F\} \\ \{Q\} \end{Bmatrix} \quad (11)$$

Where [m], [K], $[C^t]$, are the mass, stiffness, specific heat matrices, however $[K^{ut}]$ and $[C^{tu}]$ thermo-elastic stiffness damping matrices, respectively. On other side, {u}, {T}, {F} and {Q} are the displacement, temperature, force and thermal flux vectors, respectively.

The finite element models used in section 2 with coupled thermo-elastic capability in the time domain had been used to obtain the temperature profile through the thickness of the cylinder considering thermal accumulation. These results have been then used to determine the displacements in the nodes of the elements and thus the stress distribution in the cylinder. It is important to mention that the thermo-mechanical loads have been considered as radial symmetry.

RESULTS AND DISCUSSIONS

In this section, the residual stresses distribution in monoblock autofrettaged cylinder and two layers shrink-fit cylinder are firstly illustrated. Then, the temperature distribution through the wall for both cylinders is obtained due to different regimes of internal thermal loads considering thermal accumulation. Moreover, the hoop and equivalent Von-Mises stresses are obtained under combined thermo-mechanical loads (temperature and inner working pressure). Finally, the distribution of the residual stress behavior after removing the different thermo-mechanical loads and after 60 seconds of relaxation time is demonstrated.

It's important to mention that the autofrettaged cylinder, as well as the shrink-fitted one, are made of the same steel (NiCrMoV125) and the same inner and outer radii as a = 100mm and b = 200mm, respectively. The mechanical and thermal properties of the used steel are as shown in Table 1.

Table 1. Mechanical and thermal properties of cylinders' material

Young modulus	268 (GPa)	Density	7850 (kg/m^3)
yield stress	700 (MPa)	Coefficient of thermal expansion	1.7e^{-5} (1/C^o)
Tangent modulus	75(GPa)	Poisson's ratio	0.3
Thermal conductivity	43.1 (W/m. C^o)	Specific Heat	480(J/kg. C^o)

4.1 Residual Stress Distribution

The mono-block cylinder is exposed to 750 MPa internal autofrettage pressure; however, the two-layer cylinder is shrink-fitted with 0.44 mm Radial interference. That generates residual stresses in both cylinders as shown in Figure 5.

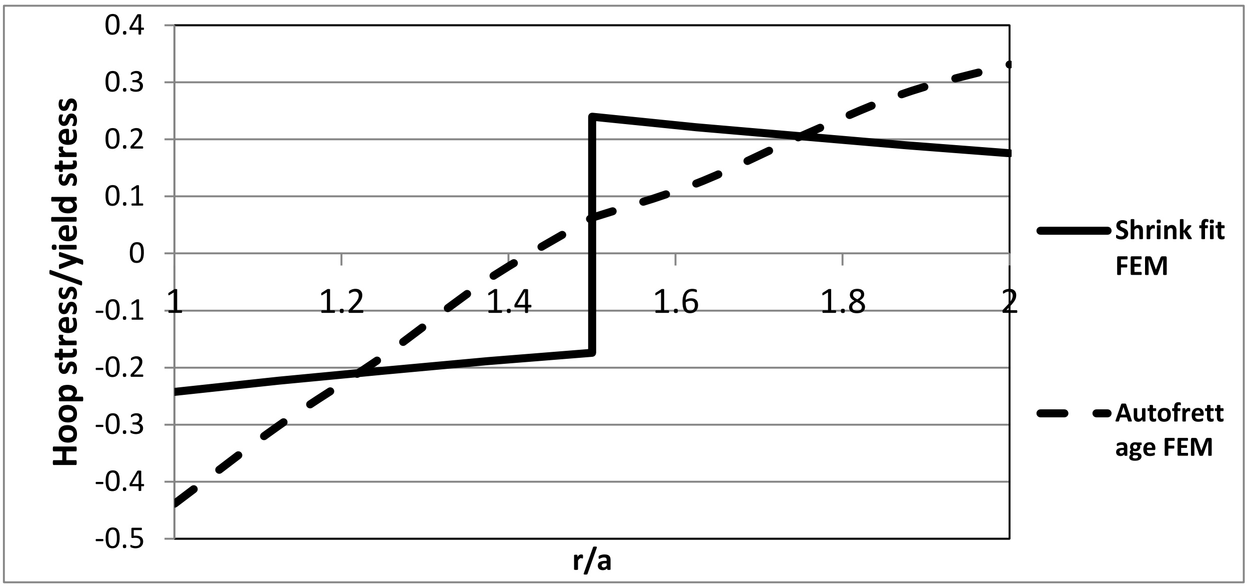

Figure 5. Residual hoop stress distribution for autofrettaged and shrink fitted cylinders

4.2 Thermal Loads and Thermal Accumulation

Thermal accumulation is one of the important concerns in dynamic thermo-mechanical cyclic loading which has to be investigated transiently in the time domain. To better realize this, the developed coupled FEM has been used to evaluate the temperature distribution in both autofrettaged and shrink-fitted cylinders when subjected to the internal cyclic heat flow as shown in Figure 6 taking into consideration thermal accumulation. As shown, each cycle has been displayed as a triangular cycle with amplitude of 1000 KW and time duration of 10 seconds each. After the cyclic loads finish, the temperature has been detected during a 60 second relaxation time.

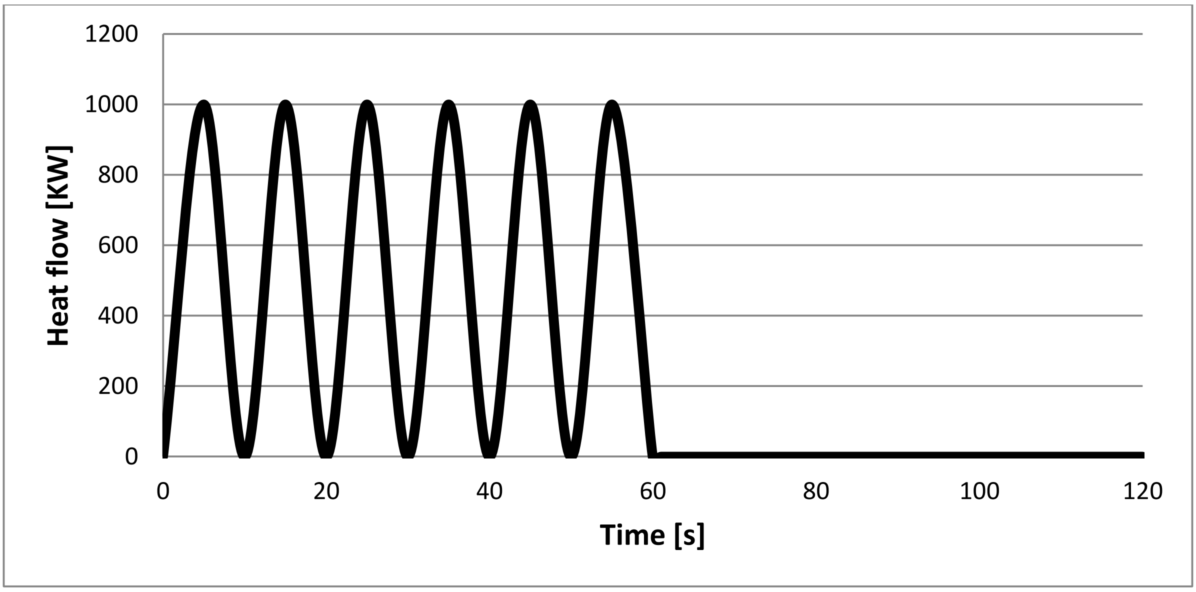

Figure 6. The internal cyclic heat flow and the relaxation time

Figures (7, 8) show the temperature distributions through the wall thickness due to the cyclic loads considering thermal accumulation and during the relaxation time considering thermal p180, respectively. It is important to mention that the temperature distribution shown has been calculated after the end of each cycle and after every 10 seconds during the relaxation time. Also, the temperature distribution is the same for both autofrettaged and shrink-fitted cylinders, as both cylinders have the same thickness and same material. The free convection boundary condition of the outer surface of the cylinders has been considered in modeling and the initial and ambient temperatures are taken as 22 ^{o}C.

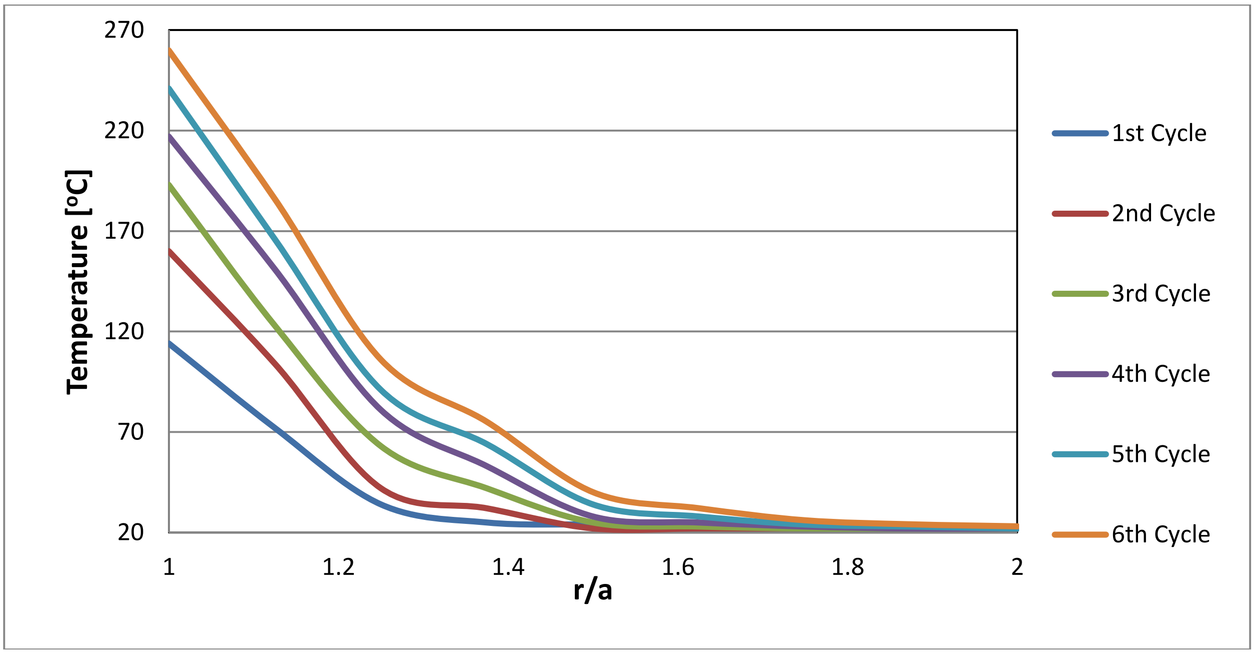

Figure 7. Temperature distribution through the wall thickness during the cyclic loads

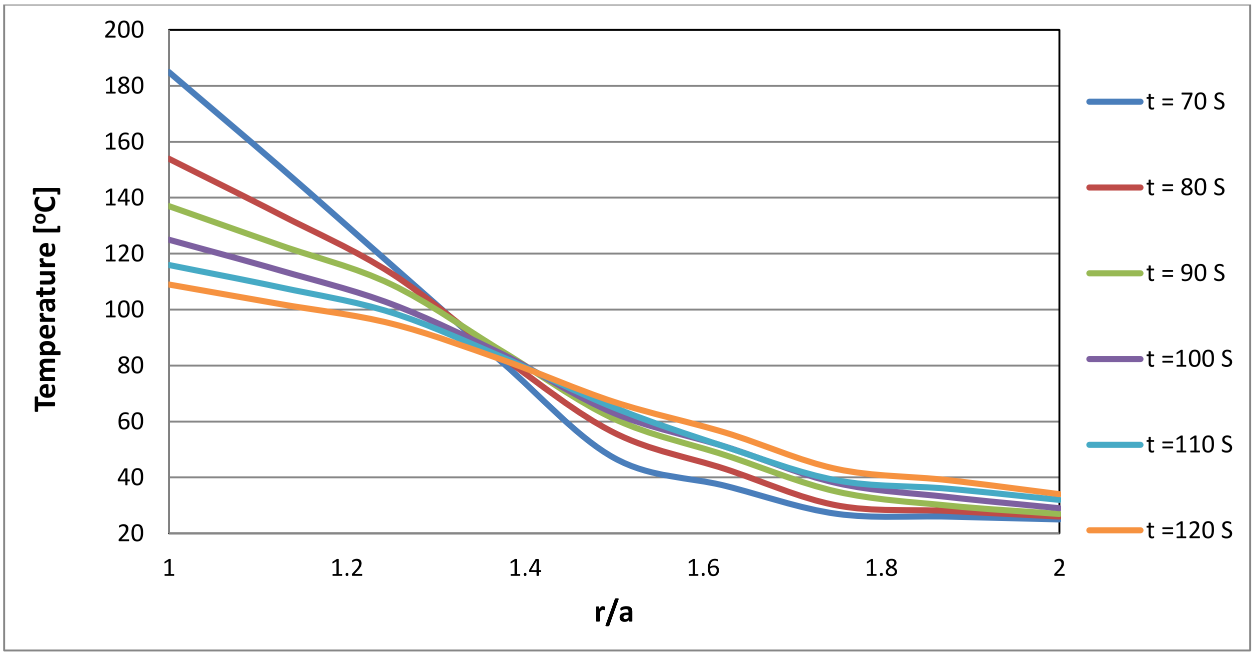

Figure 8. Temperature distribution through the wall thickness during relaxation time

4.3 Stresses due to cyclic thermo-mechanical loads

Hereinafter, the temperature distribution gained due to cyclic heat flow (as shown in Figures 7, 8) is synchronized with cyclic 350 MPa inner working pressure to be used to obtain the hoop and equivalent Von-Mises stresses. The gained stresses are calculated after each combined thermo-mechanical cycle through the wall thickness of the cylinders, as shown in Figures 9 (a, b), 10 (a, b) for the autofrettaged and shrink fitted cylinders, respectively.

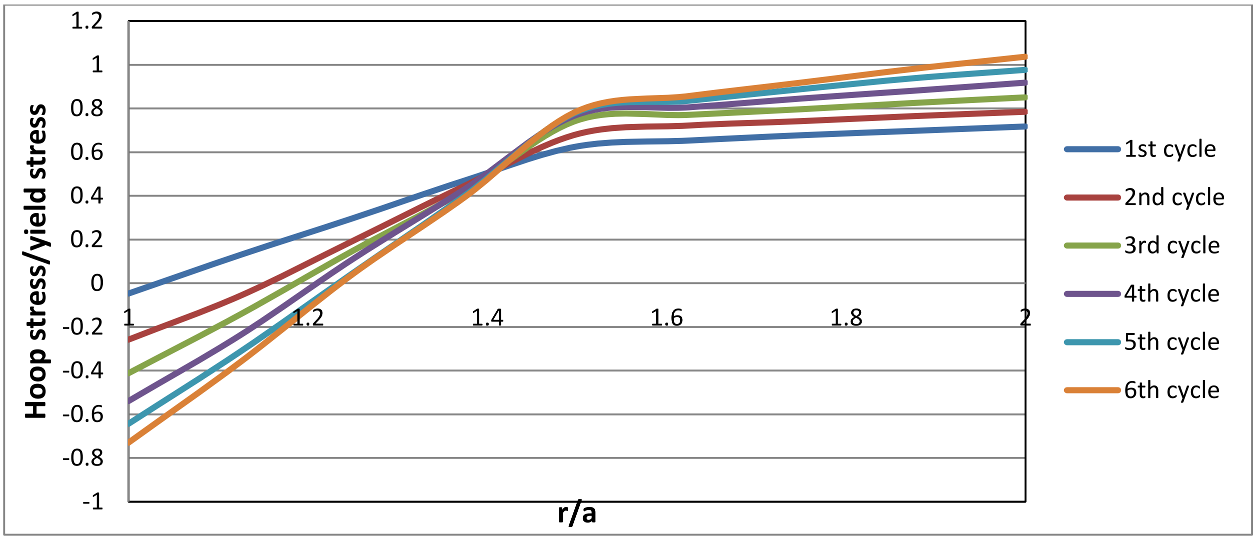

Figure 9-a. Hoop stress distribution through the wall thickness during the thermo-mechanical cycles for autofrettaged cylinder

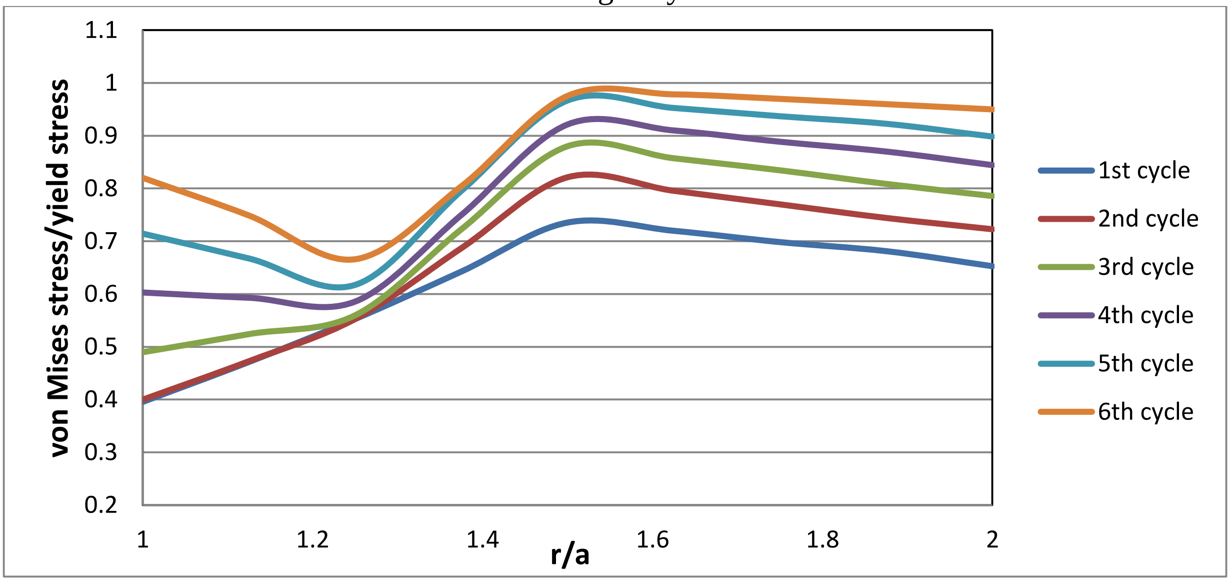

Figure 9-b. Equivalent Von-Mises stress distribution through the wall thickness during the thermo-mechanical cycles for autofrettaged cylinder

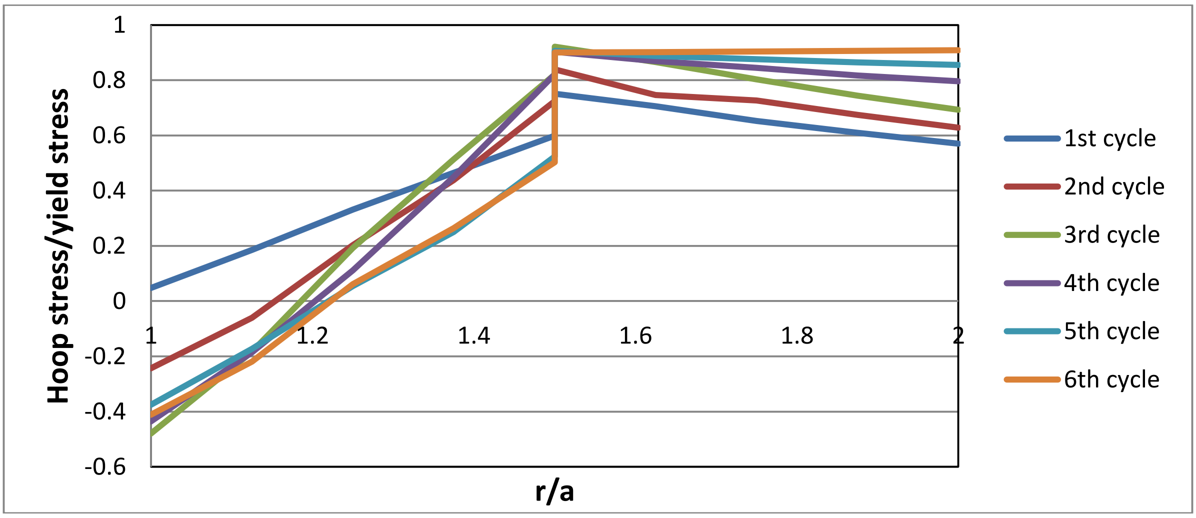

Figure 10-a. Hoop stress distribution through the wall thickness during the thermo-mechanical cycles for shrink fitted cylinder

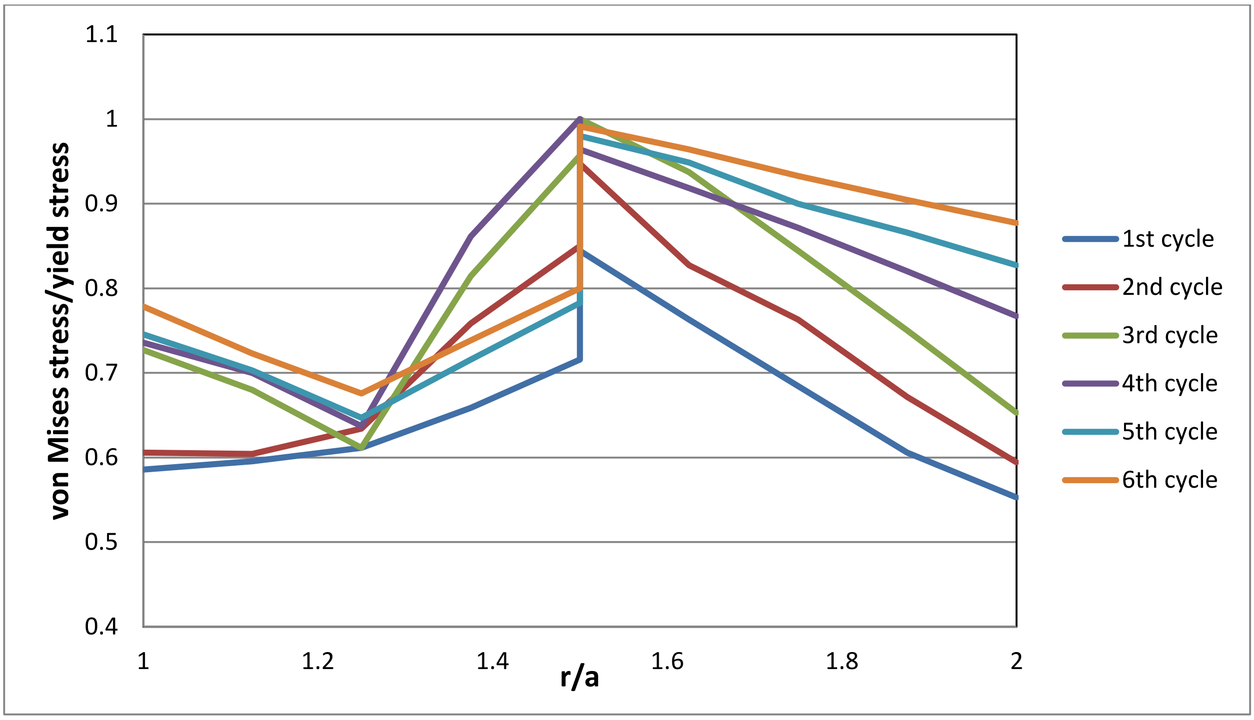

Figure 10-b. Equivalent Von-Mises stress distribution through the wall thickness during the thermo-mechanical cycles for shrink fitted cylinder

Figures (9, 10) show the effect of thermal accumulation due to cyclic thermo-mechanical loads on the hoop and equivalent stresses for autofrettage and shrink fit cylinders. It is clear in these figures that the hoop stress decreases due to thermal accumulation at the near bore area. However, it increases at the outer part of the cylinder. Consequently, the equivalent Von-Mises stresses increases obviously with thermal accumulation.

On the other hand, the residual hoop stresses are observed after every 10 seconds during the relaxation time, as shown in Figures 11, 12 for the autofrettaged and shrink-fitted cylinders, respectively. To conclude the effect of relaxation time, the original residual hoop stress has been compared with the residual hoop stress after the end of relaxation time for both autofrettage and shrink fit cylinders, as shown in Figure 13, 14, respectively.

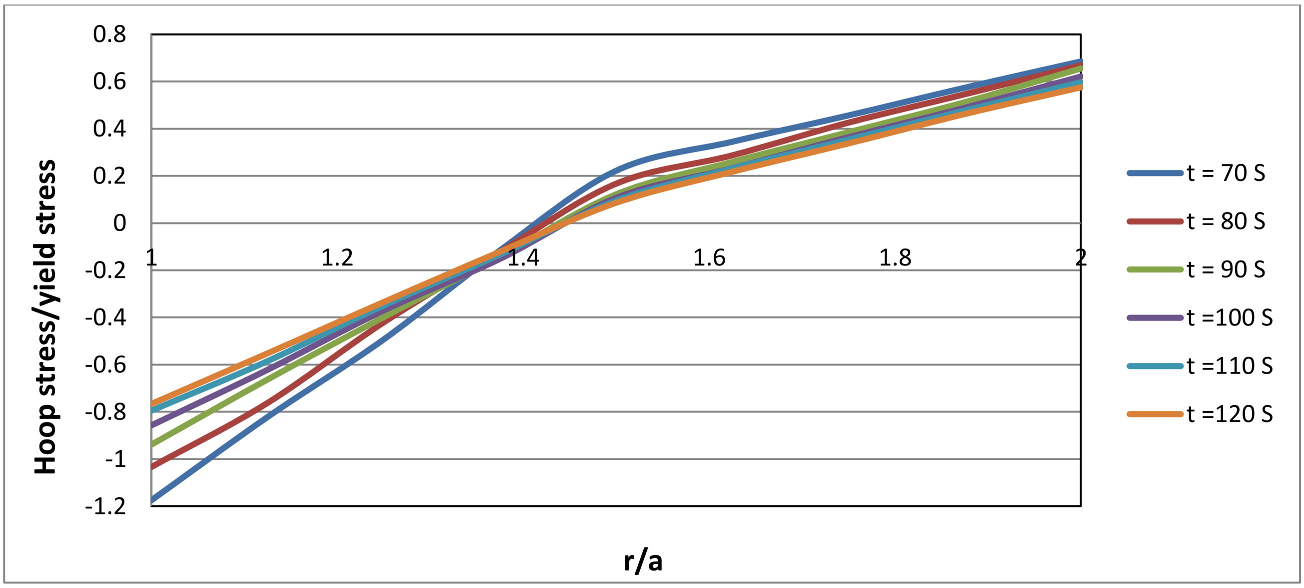

Figure 11. Hoop stress distribution through the wall thickness during the relaxation time for autofrettaged cylinder

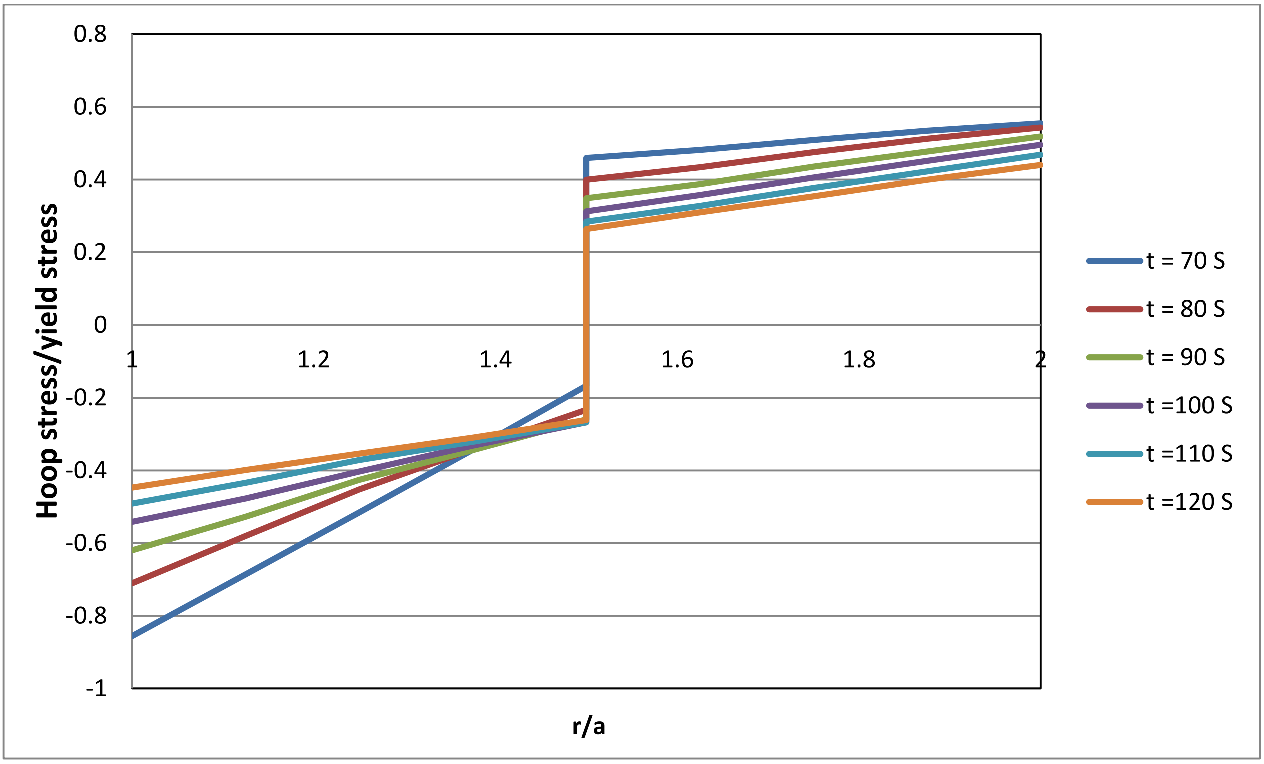

Figure 12. Hoop stress distribution through the wall thickness during the relaxation time for shrink fitted cylinder

Figures 11, 12 reveal that the residual hoop stresses observed after every 10 seconds during the relaxation time are decreased for both autofrettaged and shrink fitted cylinders and trying to return to their original values before firing.

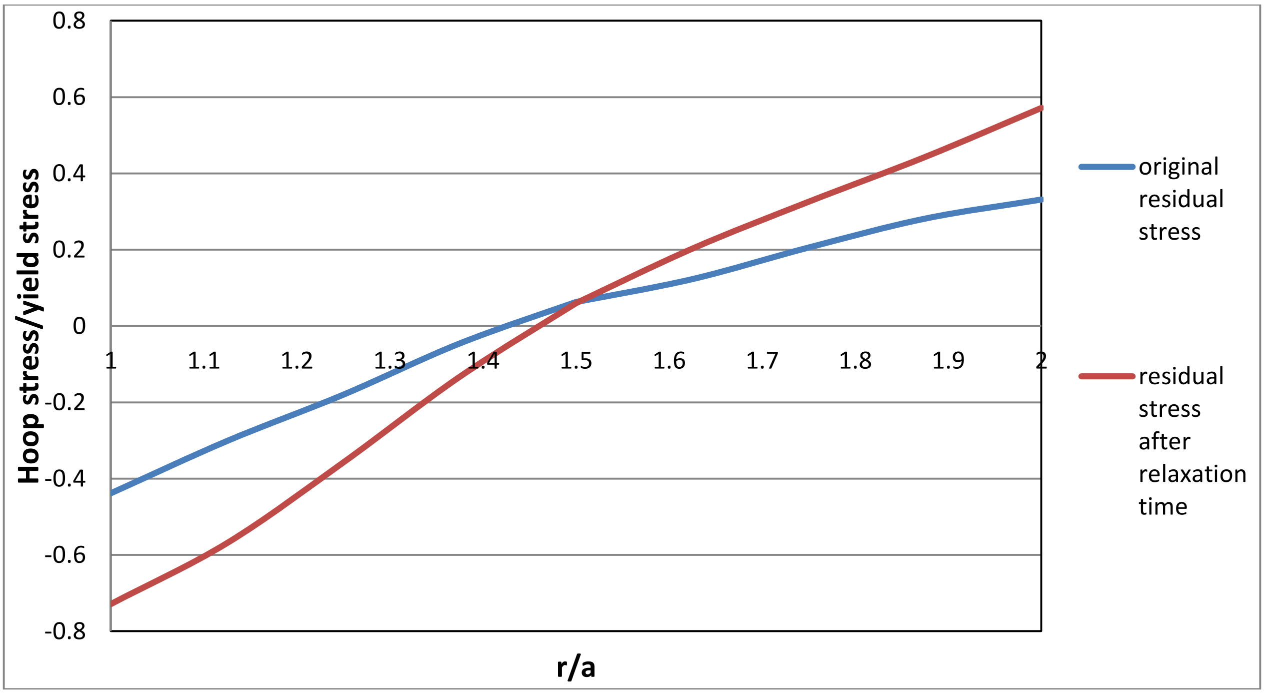

Figure 13. The original Hoop stress distribution through the wall thickness compared with that after the relaxation time for autofrettaged cylinder

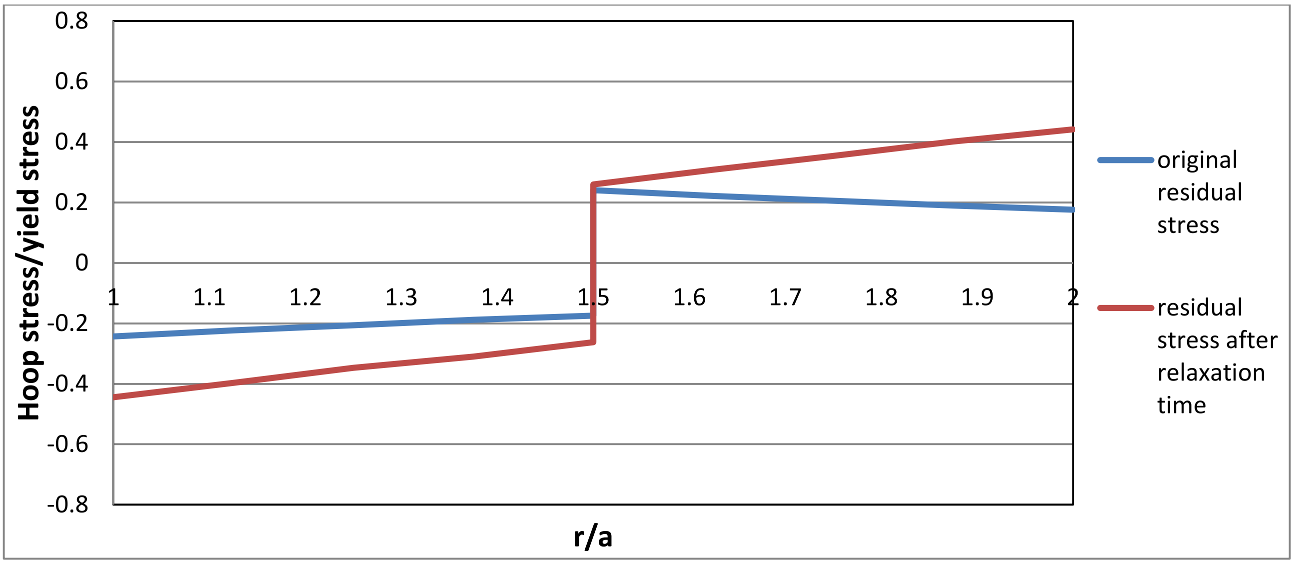

Figure 14. The original Hoop stress distribution through the wall thickness compared with that after the relaxation time for shrink fitted cylinder

For more understanding of the effect of relaxation time, the original residual hoop stress before the influence of the thermo-mechanical loads as well as the influence of thermal dissipation during the relaxation time is compared with the residual hoop stress after the end of relaxation time for both autofrettage and shrink fit cylinders, as shown in figures 13, 14. The comparison shows the importance to give the cylinders a relaxation time after the cyclic thermo-mechanical loads to return the residual stress near to its original values.

CONCLUSION

The influence of cyclic thermo-mechanical loads on the residual stress induced in autofrettaged and shrink-fitted cylinders considering thermal accumulation has been investigated. The finite Element 3D Model is first developed to evaluate the residual stresses brought by autofrettage and shrink fit processes for two different cylinders. To study the stress distribution under the effect of cyclic thermo-mechanical loads for these cylinders, a coupling 3D transient thermo-mechanical FEM was established showing the behavior of the residual stresses after these loads. Also, the effect of relaxation cooling time on the residual stresses has been observed for more than 60 seconds after the last of the thermo-mechanical cyclic loads.

The results of this study may show the following conclusions:

1- The cyclic thermal loads have a significant effect on the temperature of the cylinders, especially at the inner surfaces.

2- During relaxation time, the temperature values at the near bore area of the cylinders have been well reduced, however they increased at the outer part of the cylinder due to the continuity of conduction.

3- When the cyclic thermal load, considering thermal accumulation, is synchronized with cyclic inner working pressure, the following observations have been noted:

a- For both autofrettaged and shrink fitted cylinders, the hoop stress decreases with the thermal accumulation effect at the near bore area, however, it increases at the outer part of the cylinder.

b- For the autofrettaged cylinder, the equivalent stress increases with the thermal accumulation effect through the whole thickness of the cylinder.

c- According to the distribution of the equivalent stress, the critical part of the autofrettaged cylinder is the outer part of the cylinder; however, the critical part of shrink fitted cylinder is the interference surface of the cylinder.

4- Due to relaxation time, the hoop stress increases at the near bore area while decreases at the outer part. But finally, it comes closer to its original values before the effect of the cyclic thermo-mechanical loads. That indicates the importance of the regime of the thermo-mechanical loads as the balance between the number of cycles and relaxation time should be strongly taken into account.

REFERENCES

1) M.R. Salehi Kolahi, M. Karamooz, H. Rahmani, (2020), Elastic analysis of Shrink-fitted Thick FGM Cylinders Based on Linear Plane Elasticity Theory, Journal of Mechanics of Advanced Composite Structures, 7, 121 – 127, https://dx.doi.org/10.22075/macs.2019.18551.1221
2) Ossama R. Abdelsalam ,(2019), Design optimization for a three-layer shrink-fitted pressure vessel exposed to very high pressure, 18th International Conference on Aerospace Sciences & Aviation Technology, IOP Conf. Series: Materials Science and Engineering 610 012077 doi:10.1088/1757-899X/610/1/012077
3) Mengjun Zhao, Zhilin Wu, Hongmin Cai, (2018), Stress analyses of compound cylinders with interlayer pressure after autofrettage, International Journal of Pressure Vessels and Piping,, 163, 63-67, https://doi.org/10.1016/j.ijpvp.2018.03.002.
4) Seifi, R., (2018). Maximizing working pressure of autofrettaged three layer compound cylinders with considering Bauschinger effect and reverse yielding. Meccanica 53, 2485–2501 https://doi.org/10.1007/s11012-018-0834-2
5) Shufen, R., and Dixit, U. S. (August 2, 2018). "A Review of Theoretical and Experimental Research on Various Autofrettage Processes." ASME. J. Pressure Vessel Technol. October 140 (5): 050802. https://doi.org/10.1115/1.4039206
6) Kamal S.M., Dixit U.S., (2019), Enhancement of Fatigue Life of Thick-Walled Cylinders Through Thermal Autofrettage Combined with Shrink-Fit. In: Dixit U., Narayanan R. (eds) Strengthening and Joining by Plastic Deformation. Lecture Notes on Multidisciplinary Industrial Engineering. Springer, Singapore. https://doi.org/10.1007/978-981-13-0378-4_1
7) Zhong Hu, Anthony P. Parker, (2019), Swage autofrettage analysis – Current status and future prospects, International Journal of Pressure Vessels and Piping, 171, 233-241, ISSN 0308-0161,https://doi.org/10.1016/j.ijpvp.2019.03.007.
8) Kamal, S. M., and Perl, M. (July 15, 2019). "Generalized Plane Strain Study of Rotational Autofrettage of Thick-Walled Cylinders—Part II: Numerical Evaluation." ASME. J. Pressure Vessel Technol. October 2019; 141(5): 051202. https://doi.org/10.1115/1.4044173
9) Mohan A, Julyes Jaisingh S, Babu Aurtherson P. (2020), Fatigue analysis of thermal shrink-fit autofrettage in pressure cylinder using finite element analysis, Journal of Materials Research and Technology, 9-4, 8606-8617, https://doi.org/10.1016/j.jmrt.2020.04.021.
10) R. Shufen, U.S. Dixit, (2018), An analysis of thermal autofrettage process with heat treatment, International Journal of Mechanical Sciences, 144, 134-145, ISSN 0020-7403,https://doi.org/10.1016/j.ijmecsci..05.053.
11) Kamal, S.M., Dixit, U.S., (2016)., A comparative study of thermal and hydraulic autofrettage. J Mech Sci Technol, 30, 2483–2496 https://doi.org/10.1007/s12206-016-0508-8
12) Xue-fang Xie, Wenchun Jiang, Yun Luo, Shugen Xu, Jian-Ming Gong, Shan-Tung Tu, (2017), A model to predict the relaxation of weld residual stress by cyclic load: Experimental and finite element modeling, International Journal of Fatigue, 95, 293-301, ISSN 0142-1123,https://doi.org/10.1016/j.ijfatigue.2016.11.011.
13) Meguid, S. A., Shagal , G., Stranart, J. C., Liew , K. M., and Ong, L. S. (April 6, 2005). "Relaxation of Peening Residual Stresses Due to Cyclic Thermo-Mechanical Overload ." ASME. J. Eng. Mater. Technol. April 2005; 127(2): 170–178. https://doi.org/10.1115/1.1867986
14) ANSYS@ academic research mechanical, 2018, Theory Manual 2018, Release 18.1 Documentation, coupled field analysis, ANSYS, Inc.
15) Hamid Jahed, Behrooz Farshi, Mohammad Hosseini, (2007), The actual unloading behavior effect on thermo-mechanical stress intensity factor and life of autofrettage tubes, International Journal of Fatigue, 29-2, 360-369, ISSN 0142-1123, https://doi.org/10.1016/j.ijfatigue.2006.02.053.
16) Norton, R. L., (2011). Machine Design. Fourth edition, Prentice-Hall.
17) Allan, F. B., (2012), Applied Mechanics of Solids, CRC Press, Boca Raton, FL.
18) Altenbach, J., Altenbach, H. & Eremeyev, V.A., (2010), On generalized Cosserat-type theories of plates and shells: a short review and bibliography. Arch Appl, Mech 80, 73–92 https://doi.org/10.1007/s00419-009-0365-3